Available online at www.sciencedirect.com
SCIENCE DIRECT®
Comput. Methods Appl. Mech. Engrg. 192 (2003) 5037–5056
Computer methods in applied mechanics and engineering
www.elsevier.com/locate/cma

Development of a high-resolution hyperbolic model on quadratic elements

Tony W.H. Sheu *, P.H. Lee, R.K. Lin

Department of Engineering Science and Ocean Engineering, National Taiwan University, 73 Chow-Shan Road, Taipei, Taiwan, ROC

Received 12 September 2002; received in revised form 5 May 2003; accepted 21 July 2003

Abstract

This paper presents a class of Taylor–Galerkin (TG) finite element models on quadratic elements for solving a pure convection equation which admits discontinuities. Six parameters are introduced to preserve scheme monotonicity and control solution accuracy. In this paper we apply the M-matrix theory in the construction of monotone TG model. To avoid making the scheme overly diffusive, the flux-corrected transport (FCT) technique of Boris and Book is applied together with the underlying entropy-increasing principle and modified equation analysis developed for the TG models. Reduction of post-discontinuities is the direct use of free parameters that can make the coefficients of the even and odd derivative terms shown in the modified equation change signs alternately. Several benchmark problems are investigated to confirm the integrity of the proposed characteristic model.

Keywords: Taylor–Galerkin; Pure convection equation; Quadratic elements; Discontinuities; M-matrix theory; Entropy-increasing principle

1. Introduction

The pure advection equation has been frequently considered in the development of numerical models for gas dynamics, shallow-water hydraulics, and aeroacoustics problems [1]. In the literature, upwind finite element methods capable of suppressing convective instability include the characteristic finite element method [2], discontinuous finite element method [3], characteristic-Galerkin finite element method [4], and Petrov–Galerkin method [5,6]. In this paper the finite element model will be developed within the Taylor–Galerkin (TG) framework [7], which has been applied with great success [8,9].

When solving a non-dispersive wave equation, the discretization error will inevitably make the corresponding modified equation dispersive. The resulting numerical speed of propagation (or phase velocity) becomes a function of wave numbers [10]. Knowledge of the discrete dispersion equation is, thus, essential

* Corresponding author. Tel.: +886-2-236-25470x246; fax: +886-2-239-29885.
E-mail address: twhsheu@ntu.edu.tw (T.W.H. Sheu).

0045-7825/$ - see front matter
doi:10.1016/j.cma.2003.07.005

in the model development [11,12]. To develop a less dispersive high-order finite element model, the entropy-increasing principle and group velocity theory can be applied to minimize the dispersion error [13]. On physical grounds, entropy is not allowed to decrease in the course of wave propagation, and we employ this principle to control dispersive errors and, in turn, avoid continuous growth of the solution.

The remainder of this paper is organized as follows. Section 2 presents the essential features of the generalized TG finite element model developed on quadratic elements. This is followed by the construction of TG finite element models. In Section 4, free parameters used in the monotone TG model are determined using the M-matrix theory. In Section 5, a less dispersive high-order model is developed by virtue of the entropy-increasing principle. We then present validation results in Section 6. Finally, we draw conclusions in Section 7.

2. Some fundamentals

We study in this paper the following scalar equation:

$$\frac{\partial u}{\partial t}+\frac{\partial f}{\partial x}=0. \tag{1}$$

We assume that c shown in the physical flux term $f(u)=cu$ is a positive constant. Subject to $u(x,t=0)=\exp(\mathrm{i}kx)$, the analytic solution for Eq. (1) is derived as:

$$u_{\text{exact}}(x,t)=\exp[\mathrm{i}(kx-\omega t)], \tag{2}$$

where $S\ (\equiv kx-\omega t)$ is the phase function. In the above, k and ω denote the wave number and the frequency, respectively. The phase speed is, by definition, the speed at which the phase line advances normally to itself. As a result, $\nabla S\ (\equiv \partial S/\partial x)=k$ and $\partial S/\partial t=-\omega$. Along a phase line $S(x,t)=$ constant $(\equiv S_0)$, we have $\mathrm{d}S=\partial S/\partial t\,\mathrm{d}t+\nabla S\,\mathrm{d}x=0$ and, in turn, the phase speed $c=\frac{\omega}{k}$. This analytic dispersion relation $\omega=\omega(k)=ck$ implies that the phase speed does not depend on k. The hyperbolic equation to be investigated is, therefore, non-dispersive.

Since any numerical method may introduce dissipation and dispersion errors, the computed nodal solution at a spatial location x_j in a domain of uniform mesh size Δx is assumed to have the following form

$$u(x_j,t)=\exp\left(-c\frac{k_r}{\Delta x}t\right)\exp\left[\mathrm{i}k\left(x_j-\frac{k_i}{k\,\Delta x}ct\right)\right]. \tag{3}$$

Here, k_r and k_i are introduced to signify the dissipation and dispersion errors, respectively. The consistency property [14] requires that $k_r/\Delta x$ approach zero while $k_i/\bar{\alpha}$ approach 1, where $\bar{\alpha}=k\,\Delta x$ is defined as the modified wave number.

3. Consistent and stable quadratic Taylor–Galerkin finite element model

In this study we use the TG finite element model [7] to solve for u from the following weak equation

$$\sum_{\mathrm{el}=1}^{n_{\mathrm{el}}}\int_{\Omega^{\mathrm{el}}}\int_{t_n}^{t_{n+1}}W(x)\left(\frac{\partial u}{\partial t}+\frac{\partial f}{\partial x}\right)\mathrm{d}t\,\mathrm{d}\Omega^{\mathrm{el}}=0. \tag{4}$$

Here, the weighting function $W(x)$ has the same form as the shape function for u. As the name implies, the present model involves expanding f with respect to time t in a Taylor series and terminates the expansion to yield third-order temporal accuracy. For the purpose of controlling dissipation and dispersion errors, six parameters, α, β, γ, μ, ω and κ are employed in the expansion of f with respect to f^n

$$f = f^n + c\left(\alpha A\frac{\partial u}{\partial t} - \beta\frac{\partial f}{\partial x}\right)\Bigg|^n (t-t_n) - \frac{1}{2}c^2\left(\gamma\frac{\partial^2 u}{\partial x\,\partial t} - \mu\frac{\partial^2 f}{\partial x^2}\right)\Bigg|^n (t-t_n)^2 + \frac{1}{6}c^3\left(\omega\left(\frac{\partial u^3}{\partial x^2\,\partial t} - \kappa\frac{\partial^3 f}{\partial x^3}\right)\right)\Bigg|^n (t-t_n)^3 + \mathrm{O}((t-t_n)^4). \tag{5}$$

The remaining time derivative term is approximated by means of the Lax–Wendroff time-stepping scheme, which is

$$\frac{\partial u}{\partial t} = \frac{u^{n+1}-u^n}{\Delta t} - \frac{\Delta t}{2}\frac{\partial^2 u}{\partial t^2} - \frac{\Delta t^2}{6}\frac{\partial^3 u}{\partial t^3}. \tag{6}$$

In lieu of Eq. (1) and $f = cu$, the time derivative terms shown above can be analytically replaced by the spatial derivative terms $\frac{\partial^2 u}{\partial t^2} = -cu_{tx} = c\frac{\partial^2 f}{\partial x^2}$ and $\frac{\partial^3 u}{\partial t^3} = cf_{txx} = c^2 u_{txx} - c^2\frac{\partial^3 f}{\partial x^3}$.

Upon employing the quadratic polynomial for basis and test functions, the discretized equation for (1) at x_i can be derived in terms of the Courant number v ($\equiv \frac{u\Delta t}{2\Delta x}$) and the six introduced parameters:

$$\sum_{j=0,\pm1,\pm2} a_{i\pm j}\,\delta U^n_{i\pm j} = \sum_{j=0,\pm1,\pm2} b_{i\pm j} U^n_{i\pm j}. \tag{7}$$

In the above, $\delta U^n_{i\pm j} = U^{n+1}_{i\pm j} - U^n_{i\pm j}$. The coefficients shown above are summarized in Appendix A.

We can now derive the modified equation (second kind) for the model equation by performing Taylor series expansion on each term shown in Eq. (7). After some algebra, the following modified equation is derived:

$$u_t + cu_x = \tau_2 u_{xx} + \tau_3 u_{xxx} + \tau_4 u_{xxxx} + \cdots \tag{8}$$

The coefficients $\tau_2 \sim \tau_4$ derived at the center and corner nodes are given in Appendix B. In light of the above modified equation, the proposed finite element model is found to accommodate the consistency property [15].

We now conduct Fourier (or von Neumann) stability analysis. The amplification factor for Eq. (7) is found to have the following form:

$$G = \frac{\mathbf{a} + \mathbf{b}\mathrm{i}}{\mathbf{c} + \mathbf{d}\mathrm{i}}. \tag{9}$$

Coefficients a, b, c, and d are summarized in Appendix C. It can be shown that $|G| \leqslant 1$ no matter what the chosen parameters are. The discrete equation (7) is, therefore, unconditionally stable. Having derived a consistency-preserving finite element model, stability is the necessary and sufficient condition for convergence according to the Lax equivalence theorem [16]. Therefore, the convergent solution for (1) can be obtained using the proposed quadratic TG finite element model. Note that the convergence property can be obtained at any chosen free parameters [16].

It now remains to specify α, β, γ, μ, ω and κ for obtaining monotone (low-order) and less dispersive (high-order) solutions, which are necessary to obtain the FCT finite element solution. In the subsequent two sections, the M-matrix theory, modified equation analysis, and the entropy-increasing principle will be employed in the model development.

4. *M*-matrix finite element model

Within the FCT finite element framework, development of a high-order model in the smooth flow regime and a monotone model in the flow where discontinuities may develop is indispensable. One way of

obtaining the monotone solution for Eq. (1) is to apply the M-matrix theory [17,18]. Our derivation begins with rewriting Eq. (7) as

$$\underline{\underline{\mathbf{M}}}_{\mathrm{c}}\underline{\mathbf{u}}^{n+1} = \underline{\underline{\mathbf{C}}}\underline{\mathbf{f}} + \underline{\underline{\mathbf{M}}}_{\mathrm{c}}\underline{\mathbf{u}}^{n}. \tag{10}$$

According to Ahuès and Telias [18], a monotone solution can be obtained on condition that both $\widetilde{\underline{\underline{\mathbf{M}}}}_{\mathrm{c}}$ ($\equiv \underline{\underline{\mathbf{M}}}_{\mathrm{c}} - \underline{\underline{\mathbf{I}}}$), where $\underline{\underline{\mathbf{M}}}_{\mathrm{c}}$ and $\underline{\underline{\mathbf{I}}}$ are known as the consistent-mass matrix and identity matrix, respectively, and $\underline{\underline{\mathbf{C}}}$ shown in (10) fall into the M-matrix category. By definition, $\widetilde{\underline{\underline{\mathbf{M}}}}_{\mathrm{c}}$ is an M-matrix if the following two conditions hold:

(i) $\widetilde{\underline{\underline{\mathbf{M}}}}_{\mathrm{c}}$ is an L-matrix, which implies that $\mathrm{diag}(\widetilde{\underline{\underline{\mathbf{M}}}}_{\mathrm{c}}) \geqslant 0$ and $\mathrm{diag}(\widetilde{\underline{\underline{\mathbf{M}}}}_{\mathrm{c}}) - \widetilde{\underline{\underline{\mathbf{M}}}}_{\mathrm{c}} \geqslant 0$.

(ii) There exists a diagonal matrix $\underline{\underline{\mathbf{D}}}$ ($\equiv \mathrm{diag}(d_{ij})$) such that $\underline{\underline{\mathbf{D}}}\widetilde{\underline{\underline{\mathbf{M}}}}_{\mathrm{c}}$ is columnwise strictly diagonal dominant ($\sum_i a_{ij}d_j > 0$), or such that $\underline{\underline{\mathbf{A}}}\underline{\underline{\mathbf{D}}}$ is rowwise strictly diagonal dominant ($\sum_j a_{ij}dj > 0$).

The above two constraints guide our selection of free parameters to obtain a monotone solution at the center and corner nodes. The derivations are detailed below.

4.1. Monotone model at the center node

We first lump $b_{i\pm j}$ in (7) to obtain $b_{i+1} = b_{i-1} = 0$ and $b_i = \frac{2}{3}$. Enforcing

$$\alpha = \frac{3(\theta_1 - \theta_2)}{2v}, \tag{11}$$

$$\gamma = \frac{6 - 45\theta_1 - 45\theta_2}{40v^2}, \tag{12}$$

coefficients a_i and $a_{i\pm1}$ in (A.1)–(A.3) become $a_{i+1} = \theta_1$, $a_i = \frac{2}{3} - \theta_1 - \theta_2$, and $a_{i-1} = \theta_2$. Note that the resulting modified equation, namely, $u_t + cu_x = \tau_2 u_{x^2} + \tau_3 u_{x^3} + \tau_4 u_{x^4} + \cdots$ is obtained at

$$\theta_2 = \frac{-4v}{3} + \theta_1. \tag{13}$$

While examining the modified equation, we find that the TG model is uniformly convergent (in a sense that $\tau_2 = \tau_3 = \tau_4 = 0$ as $\Delta t \to 0$ and $\Delta x \to 0$) provided that

$$\theta_1 = -\chi v. \tag{14}$$

In the above, χ is a user's specified positive constant since θ_1 should be negative to make the discretization scheme an M-matrix type. We will set $\chi = 1$ in all the subsequent calculations. Coefficients τ_2 and τ_3 in Eq. (13) are, thus, derived as

$$\tau_2 = \frac{c\,\Delta x(5 + 4v)}{4}, \tag{15}$$

$$\tau_3 = \frac{-c\,\Delta x^2(1 + 8v^2 + 15v)}{6}. \tag{16}$$

With Eqs. (13) and (14), α and γ can be derived as follows by virtue of Eqs. (11) and (12):

$$\alpha = 2, \tag{17}$$

$$\gamma = \frac{3(1 + 25v)}{20v^2}. \tag{18}$$

At the center node, a_i and $a_{i\pm1}$ in the discrete equation can then be derived as

$$a_{i+1} = -v, \tag{19}$$

$$a_i = \frac{2(1+5v)}{3}, \tag{20}$$

$$a_{i-1} = \frac{-7v}{3}. \tag{21}$$

4.2. Monotone model at the corner node

We first lump $b_{i\pm j}$ in (7) to obtain $b_{i\pm1} = b_{i\pm2} = 0$ and $b_i = \frac{1}{3}$. Note that the bandwidth of the matrix equation is now five. More free parameters other than α and γ should be used owing to the two additional off-diagonal terms present in the matrix equation. The shortage of available free parameters motivates us to partially lump $a_{i\pm2}$ into a_i, resulting in

$$a_{i\pm2} = 0, \quad a_{i+1} = \frac{3 + 15\alpha v - 20\gamma v^2 - 15v^3\omega}{45}, \quad a_i = \frac{1}{5} + \frac{8\gamma v^2}{9} \quad \text{and}$$
$$a_{i-1} = \frac{3 - 15\alpha v - 20\gamma v^2 + 15v^3\omega}{45}.$$

The derivation is followed by conducting the analysis similar to that performed at the center nodes. The resulting free parameters are derived as

$$\alpha = 1, \tag{22}$$

$$\gamma = \frac{3(1+20v)}{20v^2}. \tag{23}$$

With α and γ thus derived, a_i and $a_{i\pm1}$, which hold at the corner node of a quadratic element, become

$$a_{i+1} = -v, \tag{24}$$

$$a_i = \frac{1+8v}{3}, \tag{25}$$

$$a_{i-1} = \frac{-5v}{3}. \tag{26}$$

The leading coefficients in the modified equation are as follows:

$$\tau_2 = c\,\Delta x(2+v), \tag{27a}$$

$$\tau_3 = \frac{-c\,\Delta x^2}{6}(1 + 8v^2 + 24v), \tag{27b}$$

$$\tau_4 = \frac{c\,\Delta x^3}{6}(1 + 26v + 48v^2 + 12v^3). \tag{27c}$$

5. High-order finite element models

5.1. Fourth/seventh-order model

According to Eqs. (B.1)–(B.3), enforcement of

$$\alpha = 1, \tag{28a}$$

$$\beta = \frac{-4 - 5v^2 + 5\kappa v^2}{5}, \tag{28b}$$

$$\gamma = \frac{-1 - 5v^2}{10v^2}, \tag{28c}$$

can eliminate the first three discretization error terms in the modified equation (8) derived at the center node. By Eqs. (B.4)–(B.6), enforcement of

$$\alpha = \frac{3(-33 + 34v^2 + 8v^4)}{14v^2(13 + 2v^2)}, \tag{29a}$$

$$\beta = \frac{-(-1881 + 7066v^2 + 1504v^4 + 16v^6)}{630v^2(13 + 2v^2)}, \tag{29b}$$

$$\gamma = \frac{-3(-53 + 58v^2 + 40v^4)}{140v^2(13 + 2v^2)}, \tag{29c}$$

$$\mu = \frac{79 + 10v^2 - 8v^4}{-156v^2 - 24v^4}, \tag{29d}$$

$$\omega = \frac{-891 + 376v^2 + 4v^4 + 16v^6}{210v^4(13 + 2v^2)}, \tag{29e}$$

$$\kappa = \frac{1287 - 6241v^2 + 7826v^4 + 1088v^6}{8190v^4 + 1260v^6}, \tag{29f}$$

can similarly eliminate the six leading discretization error terms in the modified equation at the corner node. Substituting (28a)–(28c) into (8) and (29a)–(29f) into (8), the derived τ_i in the derived modified equations at the center and corner nodes are detailed in Appendix D. In light of the derived modified equation, the orders of the proposed TG model are $O(\Delta x^4, \Delta t^4)$ at the center node and $O(\Delta x^7, \Delta t^7)$ at the corner node.

5.2. Third-order less dispersive model

We first enforce

$$\beta = \frac{1 - 5\alpha - 10v^2 + 5\alpha v^2 + 5\kappa v^2}{5} \tag{30}$$

and

$$\gamma = \frac{-(1 - 10v^2 + 15\alpha v^2)}{10v^2} \tag{31}$$

to eliminate the first two discretization error terms at the center node. By the same token, enforcement of

$$\beta = \frac{2 - 45\alpha - 20v^2 + 20\kappa v^2 + 60v^2\omega}{35}, \tag{32a}$$

$$\gamma = \frac{1 - 5\alpha - 10v^2 - 70\alpha v^2 + 45\kappa v^2 + 30v^2\omega}{70v^2}, \tag{32b}$$

$$\mu = \frac{13 + 5\alpha - 130v^2 + 280\alpha v^2 - 45\kappa v^2 - 30v^2\omega}{210v^2}, \tag{32c}$$

enables us to eliminate the three leading discretization error terms at the corner node. Substituting (30) and (31) into coefficients shown in (8), we have the coefficients shown in the modified equation at the center node:

$$\tau_2 = \tau_3 = 0, \tag{33a}$$

$$\tau_4 = \frac{-c\,\Delta x^3 v(-1+\alpha)(-1+4v^2)}{12}, \tag{33b}$$

$$\tau_5 = \frac{c\,\Delta x^4(-1+4v^2)[-1+(16-30\alpha+15\alpha^2)v^2]}{180}, \tag{33c}$$

$$\tau_6 = \frac{-c\,\Delta x^5 v(-1+\alpha)(-1+4v^2)[-1+2(4-6\alpha+3\alpha^2)v^2]}{72}. \tag{33d}$$

From (33a)–(33d), we are led to know that the modified equation varies only with α. The other three undetermined free parameters, μ, ω, and κ, have no effect on the modified equation. For simplicity, we may assign $\mu = \omega = \kappa = 0$ at the center node.

We set $\omega = \kappa = 0$ at the corner node as we did at the center node. By substituting (32) into coefficients shown in (8), at the corner node the coefficients in the modified equation can be derived as follows:

$$\tau_2 = \tau_3 = \tau_4 = 0, \tag{34a}$$

$$\tau_5 = \frac{c\,\Delta x^4[-37 - 436v^2 + 248v^4 + 5\alpha(-5 + 85v^2 + 28v^4)]}{1260}, \tag{34b}$$

$$\tau_6 = \frac{-c\,\Delta x^5 v}{1260}\left[-13 + 674v^2 - 400v^4 + 5\alpha^2(-5 + 85v^2 + 28v^4) + 2\alpha(28 - 563v^2 + 40v^4)\right]. \tag{34c}$$

Note that the accuracy order at the corner node is one order higher than that at the center node.

Subject to the initial condition given in Section 2, the exact solution to the modified equation $\frac{\partial u}{\partial t} + c\frac{\partial u}{\partial x} = \sum_{n=2}^{\infty} \tau_n \frac{\partial^n u}{\partial x^n}$ can be derived as [19]

$$u(x,t) = \mathrm{e}^{pt}\mathrm{e}^{\mathrm{i}k(x-qt)}, \tag{35}$$

where $\tau_n = k_n \Delta x^{n-1}$ and

$$p = \sum_{m=1}^{\infty} \tau_{2m}(-1)^m k^{2m}, \tag{36}$$

$$q = c - \sum_{m=1}^{\infty} \tau_{2m+1}(-1)^m k^{2m}. \tag{37}$$

Control of amplitude and propagation speed arising from the TG finite element approximation depends, thus, on τ_m and τ_{2m+1} shown in (36) and (37) and, in turn, solely on α.

To minimize the erroneous wave propagation speed and to prevent continuous growth of the amplitude error, we exploit the entropy-increasing principle [20]. On the left side of the discontinuity, we demand that

$$\sum_{m=1}^{\infty} \tau_{2m+1}(-1)^m k^{2m} < 0. \tag{38}$$

As the mesh size Δx approaches zero, $\tau_m (\equiv k_m(\Delta x)^{m-1})$ becomes negligibly small at a larger integer m. For this reason, the higher-order terms shown above can be neglected to yield the following approximated expression:

$$(-1)^m \tau_{2m+1} < 0. \tag{39}$$

On the right side of the discontinuity, we can also develop a dispersively more accurate model by enforcing

$$\sum_{m=1}^{\infty} \tau_{2m+1}(-1)^m k^{2m} > 0. \tag{40}$$

The higher-order terms shown in Eq. (40) become negligibly small as Δx approaches zero. To meet the entropy-increasing requirement, the following approximated equation can, thus, be used:

$$(-1)^m \tau_{2m+1} > 0. \tag{41}$$

In summary, Eqs. (39) and (41) guide our dispersion error reduction, in particular, in the high frequency range.

An improper specification of α can cause the TG model to be anti-dissipative. It is, thus, essential to enforce the following equation (or $e^{pt} < 1$) to make the TG model dissipative:

$$\sum_{m=1}^{\infty} \tau_{2m}(-1)^m k^{2m} < 0. \tag{42}$$

Consider only the leading term shown in the above equation; we then have

$$\tau_{2m}(-1)^m < 0. \tag{43}$$

Under these circumstances, solutions with increasing magnitude are not permitted. In what follows, α is specified according to the following two equations, which meet the constraint requirements given in (39), (41) and (43):

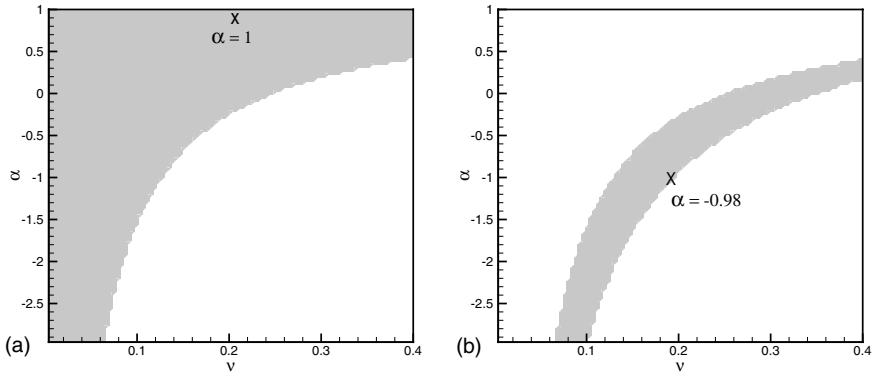

Fig. 1. The entropy-increasing regions (the sign is correct up to τ_6), obtained at $\nu = 0.2$ for the proposed model at the center node, are marked by the shaded color. (a) Ahead of the discontinuity; (b) behind the discontinuity. Note that (α, ν) marked by "×" is chosen in the calculation.

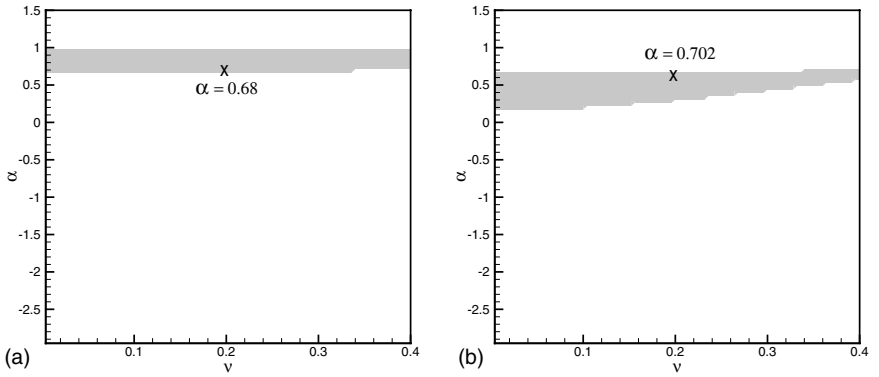

Fig. 2. The entropy-increasing regions (the sign is correct up to τ_6), obtained at $v = 0.2$ for the proposed model at the corner node, are marked by the shaded color. (a) Ahead of the discontinuity; (b) behind the discontinuity. Note that (α, v) marked by "×" is chosen in the calculation.

Table 1
Free parameters used in the M-matrix model, fourth/seventh model and entropy-increasing model

Nodal classification	Model classification							
	Low-order model		High-order models					
	M-matrix model		Fourth/seventh model		Less dispersive model			
					Ahead of the discontinuity		Behind the discontinuity	
	Center node	Corner node	Center node	Corner node	Center node	Corner node	Center node	Corner node
α	2	1	1	−12.953	1	0.68	−0.98	0.702
β	0	0	−0.84	4.841	−1	−0.68	−2.98	−0.702
γ	22.5	18.75	−3	2.073	−40.5	47.844	37.53	49.998
μ	0	0	0	−12.644	0	11.036	11.732	11.036
ω	0	0	0	−199.312	0	0	0	0
κ	0	0	0	79.634	0	0	0	0

Note that in the less dispersive model, α falls into the shaded area shown in Fig. 1 for the center node and in Fig. 2 for the corner node.

Table 2
Equation numbers for the six free parameters used in the M-matrix model, fourth/seventh model and entropy-increasing model

Nodal classification	Model classification					
	Low-order model		High-order models			
	M-matrix model		Fourth/seventh model		Less dispersive model	
	Center node	Corner node	Center node	Corner node	Center node	Corner node
α	(17)	(22)	(28a)	(29a)	–	–
β	0	0	(28b)	(29b)	(30)	(32a)
γ	(18)	(23)	(28c)	(29c)	(31)	(32b)
μ	0	0	0	(29d)	0	(32c)
ω	0	0	0	(29e)	0	0
κ	0	0	0	(29f)	0	0

Table 3
Equation numbers for the coefficients of eight leading discretization errors shown in the modified equation for the three developed models

Nodal classification	Model classification					
	Low-order model		High-order models			
	M-matrix model		Fourth/seventh model		Less dispersive model	
	Center node	Corner node	Center node	Corner node	Center node	Corner node
τ_2	(15)	(27a)	0	0	0	0
τ_3	(16)	(27b)	0	0	0	0
τ_4	–	(27c)	0	0	(33b)	0
τ_5	–	–	(D.2)	0	(33c)	(34b)
τ_6	–	–	0	0	(33d)	(34c)
τ_7	–	–	(D.3)	0	–	–
τ_8	–	–	–	(D.5)	–	–
τ_9	–	–	–	(D.6)	–	–

$$\text{ahead of the discontinuity:} \quad \tau_4 < 0, \ \ \tau_5 > 0, \ \ \tau_6 > 0, \ \ \tau_7 < 0; \tag{44}$$

$$\text{behind the discontinuity:} \quad \tau_4 < 0, \ \ \tau_5 < 0, \ \ \tau_6 > 0, \ \ \tau_7 > 0. \tag{45}$$

The regions at which the entropy-increasing principle is satisfied ahead of and behind the discontinuity are shown in Fig. 1 at the center node and in Fig. 2 at the corner node. As far as the present less dispersive model is concerned, parameters used in regions ahead of and behind the discontinuity are tabulated in Table 1. For the sake of completeness, free parameters used in the TG model and coefficients shown in the modified equations at the center and corner nodes are summarized in Tables 2 and 3.

6. Computed results

As a first step towards verifying the proposed finite element model, we will investigate the pure advection equation in $0 \leqslant x \leqslant 1$. To demonstrate different features of the proposed TG models, the problems under investigation involve smooth as well as discontinuous profiles given below

$$u(x,0) = 0.5\sqrt{1 - 100(x-0.2)^2} \tag{46a}$$

$$= 0.5 \tag{46b}$$

$$= 0.25\left[\cos\left(\frac{(x-0.8)\pi}{0.1}\right) + 1\right]. \tag{46c}$$

All the calculations were carried out at $\Delta x = 0.005$ and $\Delta t = 0.005$.

We plot first in Figs. 3–5(a) the simulated solutions obtained from M-matrix equations (17), (18) and (22), (23) for the above three investigated initial profiles. It is seen that the computed solutions are smeared at the sharply varying region but are, indeed, oscillation-free. This demonstrates the integrity of the developed monotone TG finite element model, which is critical in the development of a FCT model. We also plot the less dispersive finite element solutions. As Figs. 3(b), 4(b) and 5(b) show, the improved accuracy is, however, contaminated by oscillations in the vicinity of discontinuities. Clearly revealed by these figures is that post-discontinuity oscillations are severer than those found ahead of the shock. The advantage of using the entropy-increasing TG model is confirmed by comparing solutions plotted in Figs. 3(b), 4(b) and 5(b)

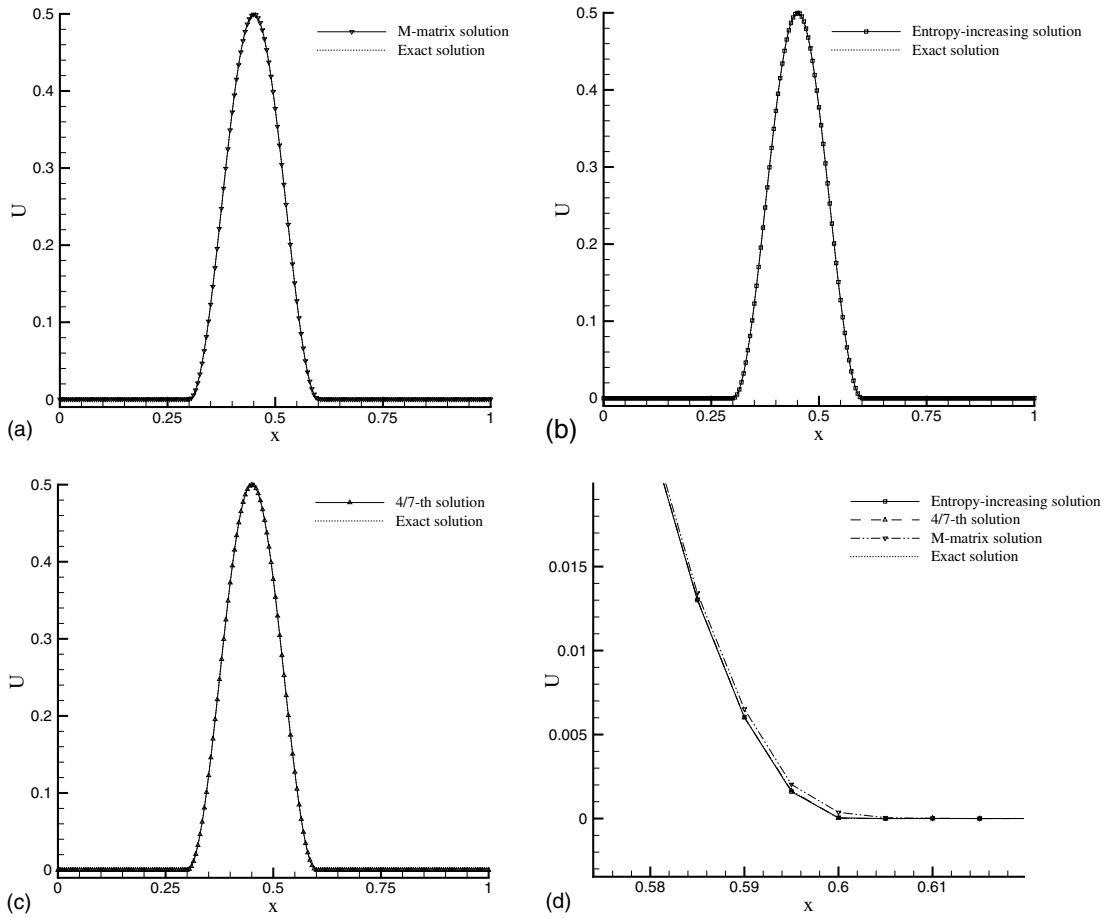

Fig. 3. Results obtained for the case involving a high gradient wave profile. (a) The computed M-matrix solution; (b) the computed entropy-increasing solution; (c) the computed fourth/seventh-order solution; (d) a close look at three solutions obtained at the bottom-right corner.

with the fourth/seventh finite element solutions plotted in Figs. 3(c), 4(c) and 5(c). Oscillations in the vicinity of discontinuity have been apparently reduced as a result of applying the less dispersive finite element model.

We also investigate a more stringent problem, subject to the initial profile defined by (46a) in $0.1 < x \leqslant 0.3$, (46b) in $0.4 < x \leqslant 0.6$, (46c) in $0.7 < x \leqslant 0.9$, and 0 elsewhere. The solutions plotted in Fig. 6 show that a non-oscillatory high-order solution can by no means be obtained from the proposed high-order TG model. For the sake of completeness, two different error norms are tabulated together with those obtained from Lax–Wendroff and Van Leer difference solutions [21,22] in Tables 4 and 5.

We now combine the monotone but diffusive model properly with the high-order model through the filtering process. Of two FCT transport solutions, FCT 1 combines the entropy-increasing and M-matrix models, while FCT 2 employs the fourth/seventh model together with the M-matrix model. A comparison of exact and simulated results is shown in Fig. 7, and the associated error norms are tabulated in Table 6. Solutions obtained from FCT 1 and FCT 2 are seen to retain the monotone property without deterioration of accuracy. This test demonstrates that the FCT model has the ability to resolve discontinuities.

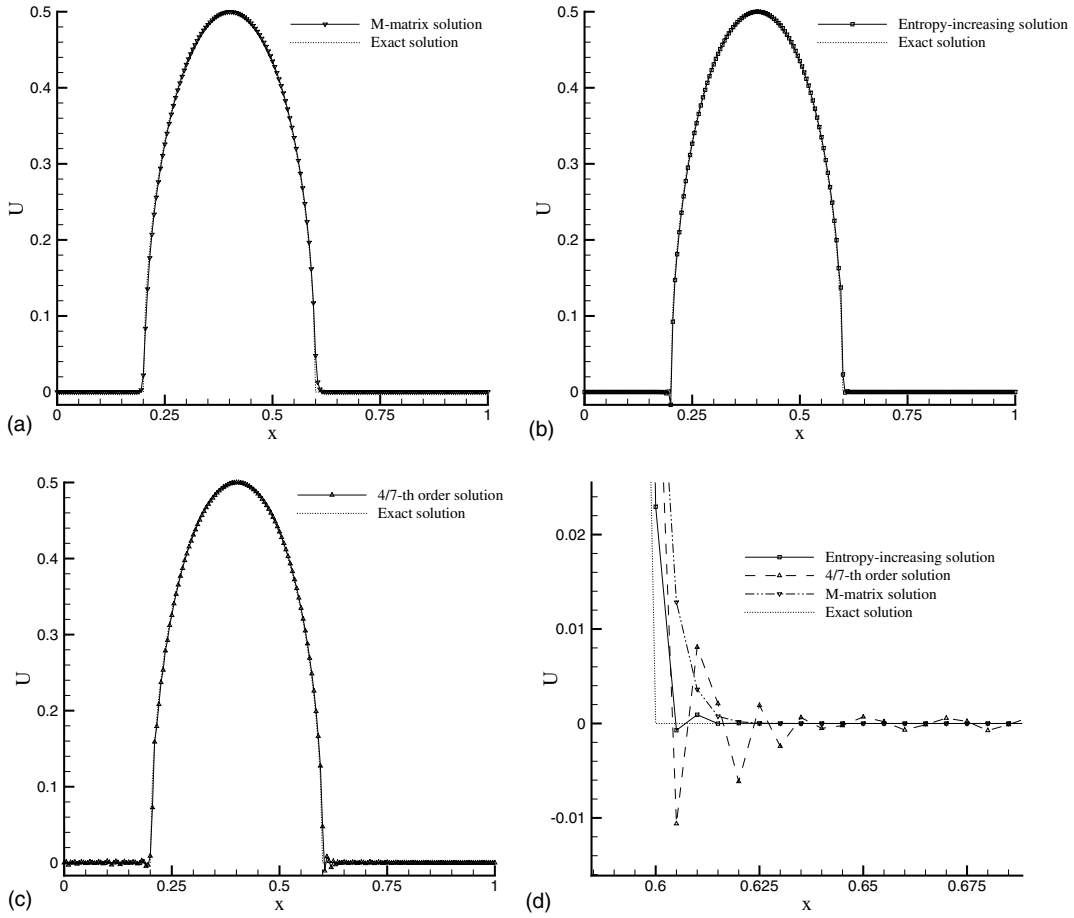

Fig. 4. Results obtained for the case involving a semi-ellipse wave profile. (a) The computed M-matrix solution; (b) the computed entropy-increasing solution; (c) the computed fourth/seventh-order solution; (d) a close look at three solutions obtained at the bottom-right corner.

The second test considers the non-linear system given by

$$u_t + uu_x = 0. \tag{47}$$

Subject to the piecewise continuous initial condition

$$u(x,0) = \begin{cases} 1 & x \leqslant 1.5, \\ 2.5 - x & 1.5 < x \leqslant 2.5, \\ 0 & x > 2.5, \end{cases} \tag{48}$$

the exact solution in $0 \leqslant x \leqslant 4$ takes the following form [23]

$$u(x, t < 1) = \begin{cases} 1 & x \leqslant 1.5 + t, \\ \dfrac{2.5 - x}{1 - t} & 1.5 + t < x \leqslant 2.5, \\ 0 & x > 2.5, \end{cases} \tag{49}$$

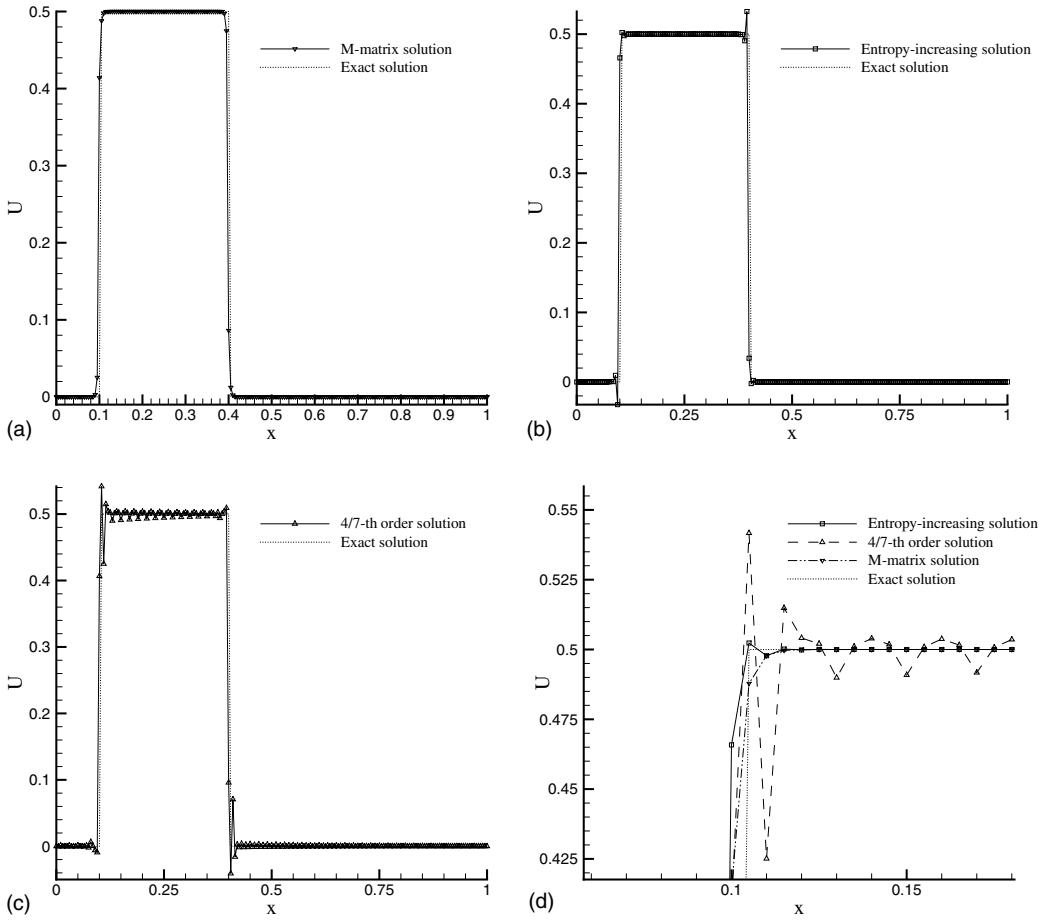

Fig. 5. Results obtained for the case involving a square wave profile. (a) The computed M-matrix solution; (b) the computed entropy-increasing solution; (c) the computed fourth/seventh-order solution; (d) a close look at three solutions obtained at the top-left corner.

and

$$u(x,t>1)=\begin{cases}1 & x\leqslant 2+0.5t,\\ 0 & x>2+0.5t.\end{cases} \tag{50}$$

Note that at $t=1$ the initially smooth solution will evolve to show a discontinuous profile at $x=0.25$ due to equation non-linearity. Non-oscillatory and monotone solutions, which were obtained at $\Delta x=0.04$ and $\Delta t=0.005$ ($v=0.125$), are shown in Fig. 8 at three arbitrarily chosen times.

7. Concluding remarks

This paper has presented a hyperbolic finite element model in quadratic elements. Six parameters introduced into the generalized TG model have been rigorously determined for obtaining physically correct and numerically accurate solutions in smoothly and sharply varying regions. Following the M-matrix

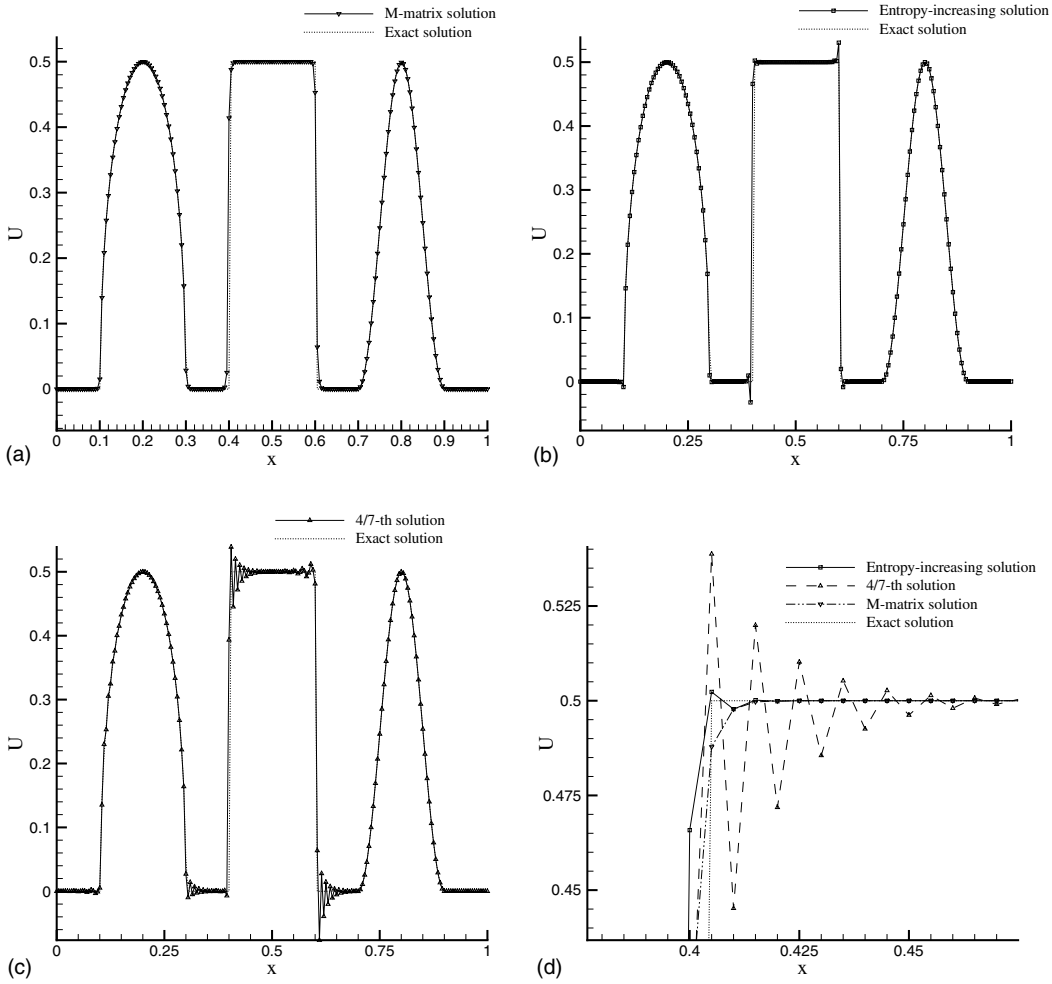

Fig. 6. Results obtained for the case involving three different wave profiles. (a) The computed M-matrix solution; (b) the computed entropy-increasing solution; (c) the computed fourth/seventh-order solution; (d) a close look at three solutions obtained at the top of center square wave.

Table 4
Error norms for models developed on the basis of modified equation analysis, the M-matrix theory and the entropy-increasing principle

Initial conditions	Error norm	Lax–Wendroff model [21]	Von Leer flux limiter model [22]	M-matrix model	Entropy-increasing model	Fourth/seventh model
Eq. (46a)	L_2	2.981×10^{-3}	3.501×10^{-4}	4.961×10^{-4}	3.719×10^{-4}	5.213×10^{-4}
Eq. (46b)	L_1	1.000×10^{-1}	6.973×10^{-1}	9.144×10^{-1}	1.033	1.331
Eq. (46c)	L_2	2.431×10^{-3}	2.472×10^{-4}	1.712×10^{-4}	5.011×10^{-5}	1.854×10^{-6}
Combined wave	L_1	2.981×10^{-1}	8.181×10^{-1}	6.911×10^{-1}	6.442×10^{-1}	1.651

For the initial conditions (46a) and (46c), L_2-norm was applied; while L_1-norm was used for profile (46b) and the combined wave case. Here, L_1- and the L_2-norms are defined as $\sum(|u_{\text{exact}}-u_{\text{numerical}}|)$ and $\sqrt{\frac{1}{\text{d.o.f.}}\sum(u_{\text{exact}}-u_{\text{numerical}})^2}$, respectively.

Table 5
Error norms for models developed on the basis of modified equation analysis, the M-matrix theory and the entropy-increasing principle

Initial conditions	Error norm	Lax–Wendroff model [21]	Von Leer flux limiter model [22]	M-matrix model	Entropy-increasing model	Fourth/seventh model
Eq. (46a)	L_2	3.012×10^{-3}	3.521×10^{-4}	5.011×10^{-4}	3.882×10^{-4}	5.618×10^{-4}
Eq. (46b)	L_1	1.010×10^{-1}	7.033×10^{-1}	9.446×10^{-1}	1.231	1.361
Eq. (46c)	L_2	2.451×10^{-3}	2.432×10^{-4}	1.927×10^{-4}	5.192×10^{-5}	2.018×10^{-6}
Combined wave	L_1	3.014×10^{-1}	8.226×10^{-1}	6.871×10^{-1}	6.371×10^{-1}	1.541

For the initial conditions (46a) and (46c), L_2-norm was applied; while L_1-norm was used for profile (46b) and the combined wave case. Here, L_1- and the L_2-norms are defined as $\int_0^T [\int_{x_L}^{x_R} |u(x,t)|\,\mathrm{d}x]\,\mathrm{d}t$ and $= \sqrt{\int_0^T [\int_{x_L}^{x_R} |u(x,t)|^2\,\mathrm{d}x]\,\mathrm{d}t}$, respectively.

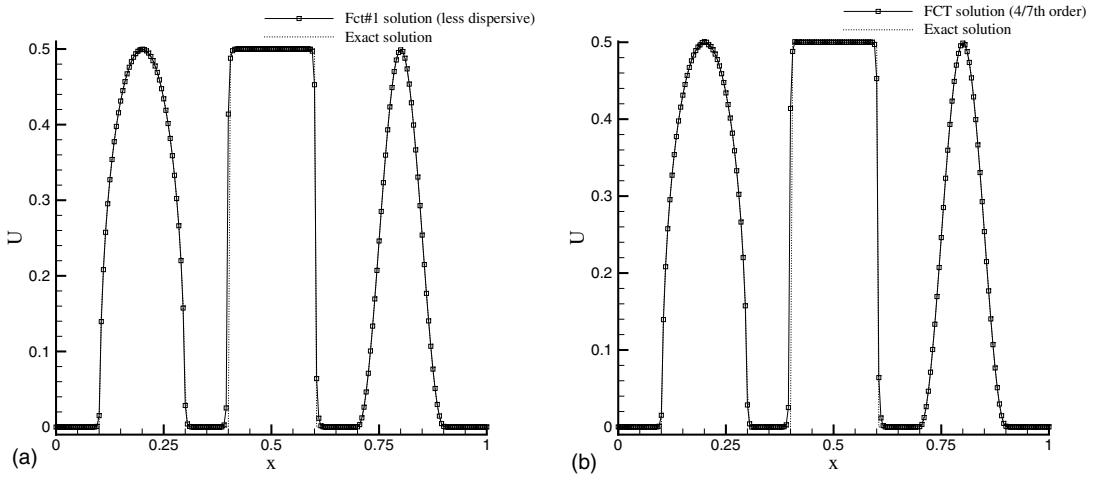

Fig. 7. Three simulated FCT solutions obtained from the (a) less dispersive model; (b) fourth/seventh-order model.

Table 6
Error norms computed using the FCT 1 and FCT 2 models for the combined wave case

Test problem	FCT 1		FCT 2	
	L_1-norm	L_2-norm	L_1-norm	L_2-norm
Combined wave (Fig. 7)	5.91×10^{-1}	3.14×10^{-2}	5.68×10^{-1}	2.99×10^{-2}

theory, the bounds for free parameters can be determined. The resulting monotonicity-preserving finite element model, while making the solution unconditionally monotone, simultaneously adds quite a large positive artificial viscosity to the non-dispersive hyperbolic system. To avoid making the model overly diffusive, two high-order finite element models, which must be built into the FCT filtering procedures, have also been rigorously developed by virtue of the respective entropy-increasing principle and modified equation analysis. Thanks to the entropy-increasing principle, in the less dispersive model we can properly control the signs of the coefficients in the leading error terms of the modified equation. Calculations have shown the integrity of all the theoretically supported TG finite element models.

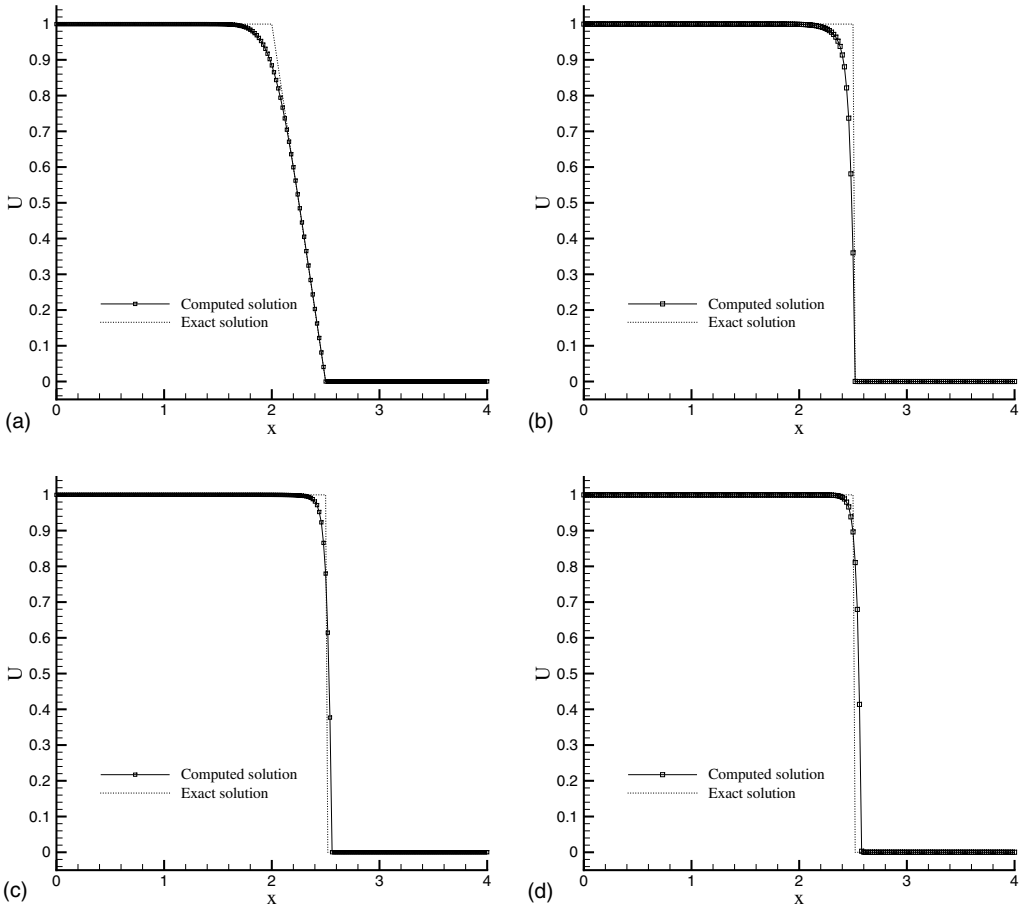

Fig. 8. The computed FCT solutions for the investigated non-linear problem at (a) $t = 0.5$; (b) $t = 1$; (c) $t = 1.5$; (d) $t = 2$.

Acknowledgements

This work was supported by the National Science Council of the Republic of China, NSC 90-2811-E-002-008.

Appendix A

The coefficients a_{ij} and b_{ij} in Eq. (7) are shown below for nodes at centered and corner points respectively.

Center node

$$a_{i+1} = \frac{1}{5} + \alpha v - \frac{4\gamma v^2}{3}, \tag{A.1}$$

$$a_i = \frac{8}{5} + \frac{8\gamma v^2}{3}, \tag{A.2}$$

$$a_{i-1} = \frac{1}{5} - \alpha v - \frac{4\gamma v^2}{3}, \tag{A.3}$$

$$b_{i+1} = -2v + 4(1+\beta)v^2 + 8\left(\alpha + \gamma - \frac{\kappa}{2}\right)v^4, \tag{A.4}$$

$$b_i = -8(1+\beta)v^2 - 16\left(\alpha + \gamma - \frac{\kappa}{2}\right)v^4, \tag{A.5}$$

$$b_{i-1} = 2v + 4(1+\beta)v^2 + 8\left(\alpha + \gamma - \frac{\kappa}{2}\right)v^4. \tag{A.6}$$

Corner node

$$a_{i+2} = \frac{1}{2}\left(-\frac{1}{5} - \frac{\alpha v}{2} + \frac{\gamma v^2}{3} + \omega v^3\right), \tag{A.7}$$

$$a_{i+1} = \frac{1}{5} + \alpha v - \frac{4\gamma v^2}{3} - \omega v^3, \tag{A.8}$$

$$a_i = \frac{4}{5} + \frac{7\gamma v^2}{3}, \tag{A.9}$$

$$a_{i-1} = \frac{1}{5} - \alpha v - \frac{4\gamma v^2}{3} + \omega v^3, \tag{A.10}$$

$$a_{i-2} = \frac{1}{2}\left(-\frac{1}{5} + \frac{\alpha v}{2} + \frac{\gamma v^2}{3} - \omega v^3\right), \tag{A.11}$$

$$b_{i+2} = \frac{v}{2} - \frac{(1+\beta)v^2}{2} - (2 - 3\alpha + 2\mu)v^3 - 4\left(\alpha + \gamma - \frac{\kappa}{2}\right)v^4, \tag{A.12}$$

$$b_{i+1} = -2v + 4(1+\beta)v^2 + 2(2 - 3\alpha + 2\mu)v^3 + 4\left(\alpha + \gamma - \frac{\kappa}{2}\right)v^4, \tag{A.13}$$

$$b_i = -7(1+\beta)v^2 - 8\left(\alpha + \gamma - \frac{\kappa}{2}\right)v^4, \tag{A.14}$$

$$b_{i-1} = 2v + 4(1+\beta)v^2 - 2(2 - 3\alpha + 2\mu)v^3 + 8\left(\alpha + \gamma - \frac{\kappa}{2}\right)v^4, \tag{A.15}$$

$$b_{i-2} = \frac{-v}{2} - \frac{(1+\beta)v^2}{2} + (2 - 3\alpha + 2\mu)v^3 - 4\left(\alpha + \gamma - \frac{\kappa}{2}\right)v^4. \tag{A.16}$$

Appendix B

The coefficients shown in Eq. (8) at the center and corner nodes are shown, respectively, below.

Center node

$$\tau_2 = c\,\Delta x v(\alpha + \beta + 2\alpha v^2 + (2\gamma - \kappa)v^2), \tag{B.1}$$

$$\tau_3 = \frac{-c\,\Delta x^2}{15}(1 + 5(-2 + 3\alpha^2 + 3\alpha(-1+\beta) - 6\beta + 2\gamma)v^2 + 15(-2+\alpha)(2\alpha + 2\gamma - \kappa)v^4), \tag{B.2}$$

$$\tau_4 = \frac{-c\Delta x^3 v}{60}(9 - 60v^2 + 60\beta^2 v^2 + 42\gamma v^2 - \kappa v^2 - 240\gamma v^4 - 80\gamma^2 v^4 + 120\kappa v^4 + 40\gamma\kappa v^4 + 240\gamma^2 v^6 - 240\gamma\kappa v^6 + 60\kappa^2 v^6 - 60\alpha^3(v^2 + 2v^4) + 60\alpha^2 v^2(2 - \beta + (8 - 2\gamma + \kappa)v^2 + 4v^4) + \beta(1 - 40(3 + \gamma)v^2 + 120(2\gamma - \kappa)v^4) + 2\alpha(-4 + (1 + 120\beta - 40\gamma)v^2 + 40(-3 + 3\beta + 5\gamma - 3\kappa)v^4 + 120(2\gamma - \kappa)v^6)). \tag{B.3}$$

Corner node

$$\tau_2 = -(c\Delta x v(-\alpha - \beta + 4\alpha v^2 + 4\gamma v^2 - 2\kappa v^2)), \tag{B.4}$$

$$\tau_3 = \frac{c\Delta x^2}{15}(2 - 5(4 + 3\alpha^2 + 3\alpha(-4 + \beta) - 6\beta + 2\gamma + 6\mu)v^2 + 30(-2 + \alpha)(2\alpha + 2\gamma - \kappa)v^4), \tag{B.5}$$

$$\tau_4 = \frac{-c\Delta x^3 v}{30}(-9 + 90v^2 + 30\beta^2 v^2 + 114\gamma v^2 - 47\kappa v^2 + 120\mu v^2 + 240\gamma v^4 + 80\gamma^2 v^4 - 120\kappa v^4 - 40\gamma\kappa v^4 + 480\gamma^2 v^6 - 480\gamma\kappa v^6 + 120\kappa^2 v^6 + 30\alpha^3 v^2(-1 + 4v^2) + 30\alpha^2 v^2(5 - \beta + (-16 + 4\gamma - 2\kappa)v^2 + 16v^4) - \beta(1 + 20(3 + \gamma)v^2 + 120(2\gamma - \kappa)v^4) + 2\alpha(4 + (-73 + 60\beta - 20\gamma - 30\mu)v^2 - 40(-3 + 3\beta + 5\gamma - 3\kappa)v^4 + 240(2\gamma - \kappa)v^6) - 30v^2\omega). \tag{B.6}$$

Appendix C

Four coefficients shown in Eq. (9) for the derived amplification factor are shown, respectively, below for nodes at the center and corner nodes.

Center node

$$\mathbf{a} = 3 + 30v - 15\alpha v + 60v^2 + 60\beta v^2 - 20\gamma v^2 + 120\alpha v^4 + 120\gamma v^4 - 60\kappa v^4 - 8\big(-3 + 5(3 + 3\beta - \gamma)v^2 + 15(2\alpha + 2\gamma - \kappa)v^4\big)\cos(\beta) + \big(3 + 15(-2 + \alpha)v + 20(3 + 3\beta - \gamma)v^2 + 60(2\alpha + 2\gamma - \kappa)v^4\big)\cos(2\beta), \tag{C.1}$$

$$\mathbf{b} = 2(-4(-3 + 5(3 + 3\beta - \gamma)v^2 + 15(2\alpha + 2\gamma - \kappa)v^4) + (3 + 15(-2 + \alpha)v + 20(3 + 3\beta - \gamma)v^2 + 60(2\alpha + 2\gamma - \kappa)v^4)\cos(\beta))\sin(\beta), \tag{C.2}$$

$$\mathbf{c} = 3 - 15\alpha v - 20\gamma v^2 + 8(3 + 5\gamma v^2)\cos(\beta) + (3 + 15\alpha v - 20\gamma v^2)\cos(2\beta), \tag{C.3}$$

$$\mathbf{d} = -2(-4(3 + 5\gamma v^2) + (-3 - 15\alpha v + 20\gamma v^2)\cos(\beta))\sin(\beta). \tag{C.4}$$

Corner node

$$\mathbf{a} = -2(-12 + 105v^2 + 105\beta v^2 - 35\gamma v^2 + 120\alpha v^4 + 120\gamma v^4 - 60\kappa v^4 - 2(3 + 20(3 + 3\beta - \gamma)v^2 + 60(2\alpha + 2\gamma - \kappa)v^4)\cos(\beta) + (3 + 5(3 + 3\beta - \gamma)v^2 + 60(2\alpha + 2\gamma - \kappa)v^4)\cos(2\beta)), \tag{C.5}$$

$$\mathbf{b} = 30v(2(-2+\alpha-6\alpha v^2+v^2(4+4\mu-\omega)) + (\alpha(-1+12v^2)+2(1+v^2(-4-4\mu+\omega)))\cos(\beta))\sin(\beta), \tag{C.6}$$

$$\mathbf{c} = 2\big(12+35\gamma v^2+(6-40\gamma v^2)\cos(\beta)-(3-5\gamma v^2)\cos(2\beta)\big), \tag{C.7}$$

$$\mathbf{d} = 30v\big(2\alpha-2v^2\omega-\alpha\cos(\beta)+2v^2\omega\cos(\beta)\big)\sin(\beta). \tag{C.8}$$

Appendix D

The coefficients of the discretization errors shown in the modified equation are shown below at the center and corner nodes, respectively.

Center node

$$\tau_2 = \tau_3 = \tau_4 = 0, \tag{D.1}$$

$$\tau_5 = \frac{c\Delta x^4(1-5v^2+4v^4)}{180}, \tag{D.2}$$

$$\tau_7 = \frac{c\Delta x^6(-1+7v^2-14v^4+8v^6)}{1512}. \tag{D.3}$$

Corner node

$$\tau_2 = \tau_3 = \tau_4 = \tau_5 = \tau_6 = \tau_7 = 0, \tag{D.4}$$

$$\tau_8 = \frac{c\Delta x^7(-891+4131v^2-1660v^4-2700v^6+1056v^8+64v^{10})}{352,800v(13+2v^2)}, \tag{D.5}$$

$$\tau_9 = \frac{c\Delta x^8}{44,452,800v^2(13+2v^2)^2}(-793,881+3,209,553v^2+545,540v^4-2,454,796v^6-1,256,176v^8 + 651,712v^{10}+93,952v^{12}+4096v^{14}). \tag{D.6}$$

References

[1] R.J. LeVeque, Numerical Methods for Conservation Laws, second ed., Birkhäaser Verlag, Basel, 1992.
[2] K.W. Morton, Generalized Galerkin methods for hyperbolic problems, Comput. Methods Appl. Mech. Engrg. 52 (1985) 847–871.
[3] P. Lesaint, P.A. Raviart, On a finite element method for solving the neutron transport problems, in: C. de Boor (Ed.), Mathematical Aspects of Finite Elements in Partial Differential Equations, Academic Press, 1974, pp. 89–123.
[4] J.H.W. Lee, J. Peraire, O.C. Zienkiewicz, The characteristic Galerkin method for advection dominated problems—an assessment, Comput. Methods Appl. Mech. Engrg. 61 (1987) 359–369.
[5] T.J.R. Hughes, M. Mallet, A. Mizukami, A new finite element formulation for computational fluid dynamics. II. Beyond SUPG, Comput. Methods Appl. Mech. Engrg. 54 (1986) 341–355.
[6] I. Christie, D.F. Griffiths, A.R. Mitchell, O.C. Zienkiewicz, Finite element methods for second order differential equations with significant first derivatives, Int. J. Num. Methods Engrg. 10 (1976) 1389–1396.
[7] J. Donea, A Taylor–Galerkin method for convective transport problems, Int. J. Num. Methods Engrg. 20 (1984) 101–119.
[8] W.W. Tworzydlo, J.T. Oden, E.A. Thornton, Adaptive implicit/explicit finite element method for compressible viscous flows, Comput. Methods Appl. Mech. Engrg. 95 (1992) 397–440.
[9] A. Safian, J.T. Oden, High-order Taylor–Galerkin method for linear hyperbolic systems, J. Comput. Phys. 120 (1995) 206–230.

[10] L.N. Trefethen, Wave Propagation and Group Velocity, Academic Press, New York, 1960.
[11] L.N. Trefethen, Group velocity in finite difference scheme, SIAM Rev. 14 (2) (1982) 113–136.
[12] B. Cathers, B.A. Óconner, The group velocity of some numerical schemes, Int. J. Numer. Methods Fluids 5 (1985) 201–224.
[13] G.F. Natter, G.E. Schneider, Use of the second law for artificial dissipation in compressible flow discrete analysis, J. Thermophys. Heat Transfer 8 (3) (1994) 500–506.
[14] P.D. Lax, Hyperbolic System of Conservation Laws and the Mathematical Theory of Shock Waves, Society for Industrial and Applied Mathematics, Philadelphia, PA, 1973.
[15] R.F. Warming, B.J. Hyett, The modified equation approach to the stability and accuracy analysis of finite difference methods, J. Comput. Phys. 14 (1974) 159–179.
[16] P.D. Lax, Week solutions of nonlinear hyperbolic equations and their numerical computation, Comm. Pure Appl. Math. 2 (1954) 159–193.
[17] T. Meis, U. Marcowitz, Numerical Solution of Partial Differential Equations, Applied Mathematical Sciences, vol. 32, Springer-Verlag, New York, 1981.
[18] M. Ahués, M. Telias, Petrov–Galerkin scheme for the steady state convection diffusion equation, Finite Elements Water Resour. 2/3 (1982).
[19] Tony W.H. Sheu, P.H. Lee, A theoretical Taylor–Galerkin model for first-order hyperbolic equation, Int. J. Numer. Methods Fluids 42 (2003) 439–463.
[20] H. Zhang, Q. Lee, F. Zhuang, On the construction of high order accuracy difference schemes, ACTA Aerodynam. Sin. 16 (1) (1998) 14–23.
[21] P.P. Lax, B. Wendroff, Systems of conservation laws, Commun. Pure Appl. Math. 13 (1960) 217–237.
[22] B. van Leer, Towards the ultimate conservative difference scheme. V. A second-order sequel to Godunov's method, J. Comput. Phys. 32 (1979) 101–136.
[23] B.R. Shin, T. Ikohagi, H. Daiguji, A modified QUICK scheme with good stability and high convergence rate, Comput. Fluid Dynam. J. 7 (3) (1998) 283–299.